Interface reconstruction strategy enabling the efficient light-driven amination of furfuryl alcohol

Yaorong He, Xiao Wang, Shanshan Ou, Lin Zhu, Tong Su, Rongfang Zhang, Wei Zhao, Hui Huang, Zhiqiang Wang, Peiyao Du, Xiaoquan Lu**

Table of Contents

Experimental Section

1. Chemical reagents and instruments

Aluminum nitrate nonahydrate ($Al(NO_3)_3·9H_2O$, 99.0%), ammonium hydroxide ($NH_3·H_2O$, 99.999%, 28% in H_2O), and 5,5-dimethyl-1-pyrroline-N-oxide (DMPO, 97%) were purchased from Shanghai Aladdin Biochemical Technology Co., Ltd. Additionally, cobalt(II) nitrate hexahydrate ($Co(NO_3)_2·6H_2O$, 98%), potassium ferricyanide ($K_3Fe(CN)_6$, 99%), cadmium nitrate tetrahydrate ($Cd(NO_3)_2·4H_2O$, 99%), urea (99%), furfuryl alcohol (98%), furfural (99%), furfurylamine (98%), and Nafion perfluorinated resin solution (5% w/w in water) were sourced from Shanghai Sane Chemical Technology Co., Ltd. Ethylenediamine (AR), formic acid (AR), ethanol (AR), and acetone (AR) were obtained from Chengdu Kelong Chemical Co., Ltd. Sodium hydroxide (NaOH, AR), ethylene glycol (AR), sodium sulfate (Na_2SO_4, AR), and potassium chloride (KCl, AR) were acquired from Guangdong Guanghua Sci-Tech Co., Ltd.

The morphology and microstructure of materials were characterized using a transmission electron microscope (TEM, Hitachi HT7800). High-resolution TEM (HRTEM) and energy-dispersive X-ray spectroscopy (EDX) were conducted with a FEI Talos F200X. The crystalline structures of the samples were identified through X-ray diffraction analysis (XRD) using a Bruker D8 ADVANCE A25. The optical absorptance of the samples was obtained with a UV-visible diffuse reflectance spectrometer (DRS), employing a UV-2600i from Shimadzu, Japan, with $BaSO_4$ as the reflectance standard. The relative amount of each element was determined with an inductively coupled plasma optical emission spectrometer (ICP-OES) from Macylab Instruments Inc., Shanghai, China (ICP-6800). A Raman spectrometer, the LabRAM HR Evolution from HORIBA, was used with an excitation laser wavelength of 532 nm. X-ray photoelectron spectroscopy (XPS) was performed on a Shimadzu/KRATOS Axis Ultra DLD spectrometer to determine the surface composition of the sample and the electron binding energy of each element, utilizing a monochromatic Al Kα X-ray source. In situ DRIFTS measurements were performed on Bruker INVENIO S infrared spectrometer.

2. Preparation of materials

Preparation of CdS Nanorods

The CdS nanorods[1] were prepared using a simple solvothermal method. A total of 1.9280 g of $Cd(NO_3)_3·4H_2O$ were dissolved in 35 mL of ethanediamine under vigorous magnetic stirring. Subsequently, 1.4273 g of thiourea were added. After stirring for 20 min, the mixture was transferred into a Teflon-lined stainless-steel autoclave and heated, maintaining the temperature at 160 °C for 20 h. Upon natural cooling, a yellow precipitate was collected by centrifugation, washed several times with deionized water and ethanol, and then dried in a vacuum oven.

Preparation of $CdS/CoAl(OH)_x$

A specific amount of as-prepared CdS nanorods (10, 25, 50, 75, or 100 mg) was added to 10 mL of ethylene glycol. Following 30 min of ultrasonic treatment at room temperature, 0.6 mL of 0.05 mM $Co(NO_3)_2·6H_2O$, 0.025 mM $Al(NO_3)_3·9H_2O$, and 0.375 mM urea were introduced into the suspension. The mixture was then stirred for 30 min before being transferred into a 25 mL autoclave and heated to 120 °C for 10 h. After cooling naturally, the product ($CdS/CoAl(OH)_x$) was collected via centrifugation and washed three times with deionized water and ethanol. The obtained products were dried in a vacuum oven.

$CdS/Co(OH)_x$ was synthesized using the same procedure as $CdS/CoAl(OH)_x$, with the exception of omitting $Al(NO_3)_3·9H_2O$.

Preparation of $CdS/CoAl(OH)_x$-R

$CdS/CoAl(OH)_x$ (50 mg) was added to 2 M NaOH aqueous solution and stirred at 100 °C for 30 min to selectively remove Al from $CoAl(OH)_x$, resulting in the reconstructed $CoAl(OH)_x$. The as-prepared product was then centrifuged and washed with deionized water until it reached a neutral pH. The resulting product, $CdS/CoAl(OH)_x$-R, was dried in a vacuum oven. Samples were prepared with varying reconstruction times (10, 20, 30, 40 min) using the same procedure.

3. Photocatalytic experiments and product analysis

Photocatalytic furfuryl alcohol to furfurylamine

The performance of the as-prepared photocatalysts in the production of furfurylamine was investigated using a top-irradiation setup with a 300 W Xe lamp (PLS-SXE300+, Perfect Light). In a typical experiment, 10 mg of photocatalyst was dispersed by constant stirring in 20 ml of a mixed solution containing 1 mmol of substrate, 1 mmol of formic acid, 5 ml of a 28 wt% ammonia solution, and ultra-pure water. Prior to the reaction, the suspension was purged with argon for 30 min to create an oxygen-free environment. The visible light-driven photocatalytic reaction was then conducted at room temperature under 1 bar of argon for 10 h. The filtered product was analyzed using high-performance liquid chromatography (HPLC, Shimadzu LC-2060C) equipped with a diode array detector. The mobile phase consisted of a 0.1% trifluoroacetic acid (TFA) aqueous solution and MeCN (70%:30%) at 35 °C. The furfurylamine was analyzed on a Shim-pack GISS C18 column (4.6×250 mm).

Photocatalytic H_2-production test

The photocatalytic hydrogen (H_2) evolution test was conducted using a 300 W Xe lamp. Typically, 10 mg of catalyst was suspended in 40 ml of a mixed solution containing 2 mmol of lactic acid and deaerated water. Prior to the reaction, the suspension was purged with argon for 30 min to create an oxygen-free environment, and the visible light-driven photocatalytic reaction was carried out at room temperature. The H_2 content was analyzed using gas chromatography (Fuli GC-9790, equipped with a thermal conductivity detector

TCD, using N_2 as the carrier gas).

4. Calculation methods of selectivity, conversion, and yield

$$Selectivity\ (\%) = \left[\frac{C_0 - C_r}{C_0}\right] \times 100\% \qquad \text{Eq. 1}$$

$$Conversion\ (\%) = \left[\frac{C_p}{C_0 - C_r}\right] \times 100\% \qquad \text{Eq. 2}$$

C_0 denotes the initial concentration of reactants, and the concentration of reactants and products after a certain period of the photocatalytic reaction is denoted by C_r and C_p, respectively.

5. Free radical test

Firstly, 5 mg of CdS/CoAl(OH)$_x$-R was dispersed in the mixture of 1 mL of DI water and 10 μL of 5,5-dimethyl1-pyrroline N-oxide (DMPO). The electron paramagnetic resonance signals for hydroxyl radical were obtained under light for 5 min. In addition, the carbon-centered radical signal was detected under the same test conditions, except that 21 μL of FFA and 100 μL $NH_3 \cdot H_2O$.

6. Photoelectrochemical (PEC) measurements

The electrochemical and photoelectrochemical (PEC) performances were investigated using an electrochemical workstation (CHI760E, Shanghai Chenhua Instrument Co., Ltd., Shanghai, China) with a standard three-electrode cell. Typically, the reference electrode was Ag/AgCl, the counter electrode was a platinum wire, and the working electrodes were prepared as follows: 2.5 mg of the sample was dispersed in a mixture of 125 μL of ultrapure water, 125 μL of ethanol, and 10 μL of Nafion solution, and followed by ultrasonic treatment to form a homogeneous ink for 30 min. Subsequently, the ink was dropped onto the pre-cleaned 1 cm × 1 cm FTO glass electrode surface and air-dried prior to measurement. The transient photocurrent spectrum was recorded at a potential of 0.5 V vs Ag/AgCl in a 0.5 M Na_2SO_4 solution. Electrochemical impedance spectroscopy was conducted at an AC amplitude of 50 mV in 0.5 M Na_2SO_4 solution under AM 1.5G illumination, with a frequency range from 0.1 Hz to 10 kHz.

Hg/HgO and Ag/AgCl reference electrodes were employed for electrochemical measurements in alkaline and neutral environments, respectively. The experimental electrode potential versus Hg/HgO was converted to the potential versus reversible hydrogen electrode (RHE) according to the following Nernst equation[2]:

$$E_{\mathrm{RHE}} = E_{\mathrm{Hg/HgO}} + 0.059\mathrm{pH} + 0.098 \qquad \text{Eq. 3}$$

The conversion of Ag/AgCl (saturated KCl) reference electrode to RHE is expressed as the following equation:

$$E_{\mathrm{RHE}} = E_{\mathrm{Ag/AgCl}} + 0.059\mathrm{pH} + 0.198 \qquad \text{Eq. 4}$$

Time-correlated open-circuit potential decay curves (OCP) were measured in 0.5 M Na_2SO_4. The OCP after the light is turned off represents the surface charge recombination behavior of trapped carriers, simulating the photogenerated carrier recombination behavior in a photocatalyst without an external applied bias. The average surface recombination rate can be estimated by fitting the data to a first-order kinetic model[3].

$$\frac{E - E_{pH}}{E_0 - E_{pH}} = 1 - e^{-K_r t} \qquad \text{Eq. 5}$$

where E represents the open-circuit potential at any given time, E_0 denotes the stationary OCP value in darkness, E_{pH} signifies the photostationary OCP value, and K_r is the pseudo-first-order recombination rate constant. Consequently, the fitted recombination rate constants are presented in Table S4.

Mott-Schottky (M-S) plots were recorded at a frequency of 1000 Hz in the dark. The donor densities (N_d) of the sample are calculated according to the Mott-Schottky equation[4] (Eq. 6).

$$N_d = \left(\frac{2}{e_0 \varepsilon \varepsilon_0 \varepsilon}\right) \cdot \left[\frac{d\left(\frac{1}{C^2}\right)}{dV}\right]^{-1} \qquad \text{Eq. 6}$$

where e_0 is the electron charge (1.60×10^{-19} C), ε is the dielectric constant of semiconductor (38 for CdS NRs), ε_0 is the permittivity of vacuum (8.85×10^{-14} F cm^{-1}), C is the capacitance of the depletion region, V is the applied voltage, and $d(1/C^2)/dV$ is the slope of Mott-Schottky plot.

Intensity-modulated photocurrent spectroscopy was tested at an applied potential of 0 V versus Ag/AgCl in 0.5 M Na_2SO_4, using a LED array (450 nm) as the light source. The transient time (τ_d) value can be calculated according to Eq. 7[5].

$$\tau_{\mathrm{d}} = \frac{1}{2\pi f_{min}} \qquad \text{Eq. 7}$$

where f_{min} was the characteristic minimum frequency at the lowest point of IMPS plot. Meanwhile, the rate constants of charge recombination (K_{re}) and transfer (K_{ct}) were calculated using the following formulas[6]:

$$\frac{I_{\text{steady state}}}{I_{\text{transient state}}} = \frac{K_{ct}}{K_{ct}+K_{re}} \times 100\% \quad \text{Eq. 8}$$

$$K_{ct} + K_{re} = 2\pi f_{max} \quad \text{Eq. 9}$$

where f_{max} was the characteristic maximum frequency at the highest point of IMPS plot.

7. Scanning photoelectrochemical microscopy measurements

Scanning photoelectrochemical microscopy (SPECM) measurements were conducted following the methodology reported by our group[7]. The SPECM setup is designed with a four-electrode system, which includes platinum wire as the counter electrode, an Ag/AgCl electrode as the reference electrode, an ultramicroelectrode (UME, RG≈ 3) with a diameter of 25 μm serving as the working electrode 1 (WE1), and substrate electrodes with specific samples acting as working electrode 2 (WE2). The potential of the UME and substrate electrode were selected at 0.15 V and 0 V versus Ag/AgCl, respectively. All electrodes were immersed in an electrolyte containing 1 mM $K_3Fe(CN)_6$ and 0.1 M KCl. The light source was a 300 W Xe lamp. This light is directed towards the surface of the photoanode along the optical pathway. During the SPECM operation, the tip current (i_T) was obtained by applying the reduction or oxidation potential to the UME. The feedback mode was used to investigate the charge transfer kinetics. Additionally, the normalized current I_T is plotted against the normalized distance L. The normalized tip current, I_T, was calculated according to the following equation:

$$I_T = i_T / i_{T,\infty} \quad \text{Eq. 10}$$

where i_T was the real-time current as the tip approaches the substrate, and $i_{T,\infty}$ is a constant value obtained when the tip is far from the substrate.

The normalized distance L was calculated according to the following equation:

$$L = d/a \quad \text{Eq. 11}$$

where d is the real-time distance between the tip and substrate electrode, and a is the radius of the tip electrode. The rate constant (K_{eff}) can be calculated from the experimental simulation. The mappings were obtained in constant height mode on a small scale (80 × 80 μm).

Results and Discussion

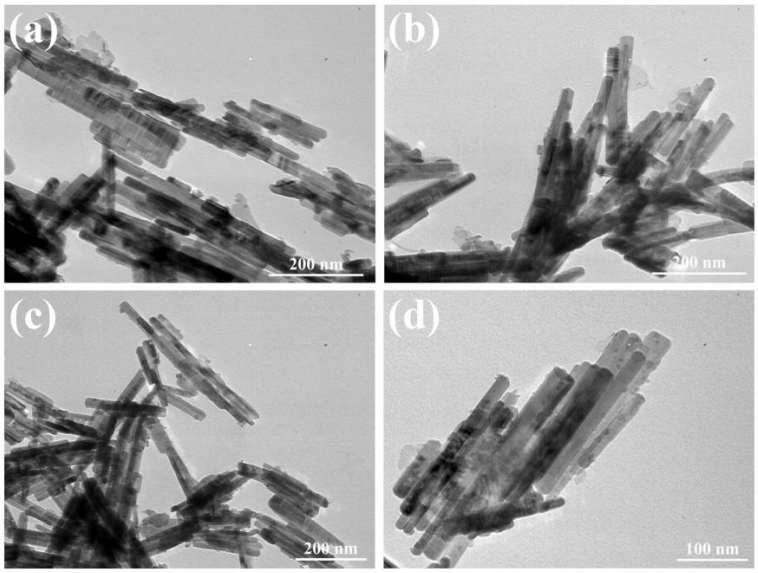

Figure S1 TEM images of CdS/CoAl(OH)$_x$ nanorods with varying alkali etching times.

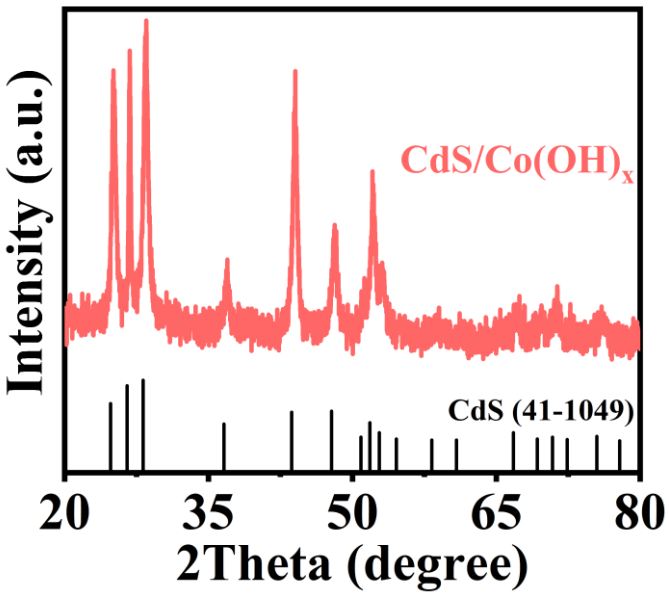

Figure S2 XRD pattern of $CdS/Co(OH)_x$.

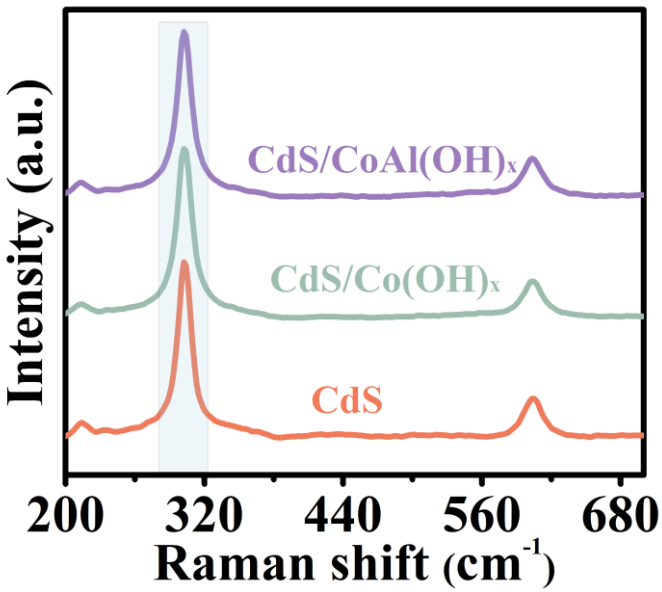

Figure S3 Raman spectra of CdS, CdS/Co(OH)$_x$, and CdS/CoAl(OH)$_x$.

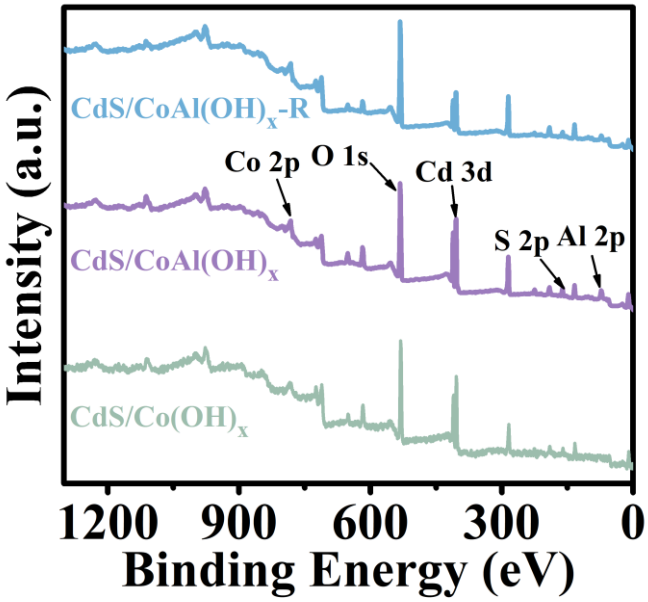

Figure S4 XPS survey spectra of CdS/Co(OH)$_x$, CdS/CoAl(OH)$_x$, and CdS/CoAl(OH)$_x$-R.

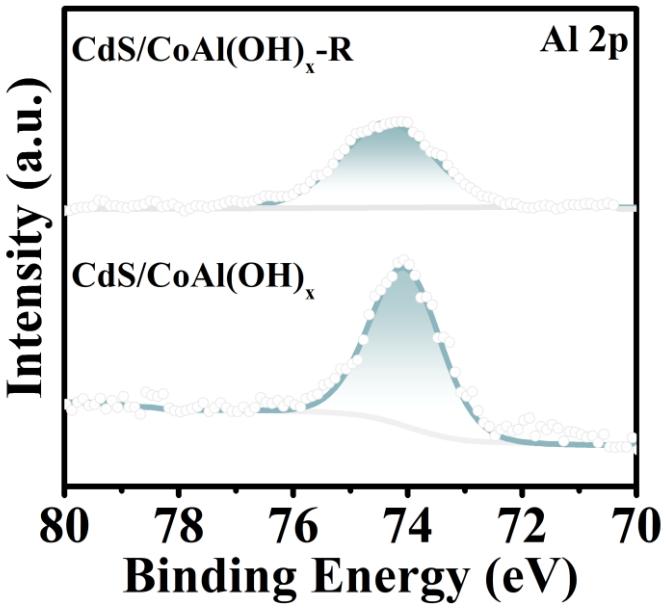

Figure S5 High resolution XPS spectra of Al 2p.

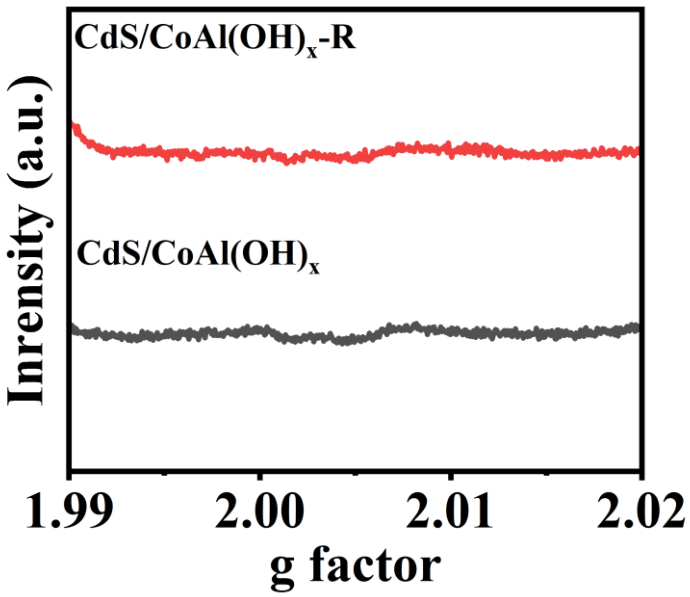

Figure S6 EPR spectra of $CdS/CoAl(OH)_x$ and $CdS/CoAl(OH)_x$-R.

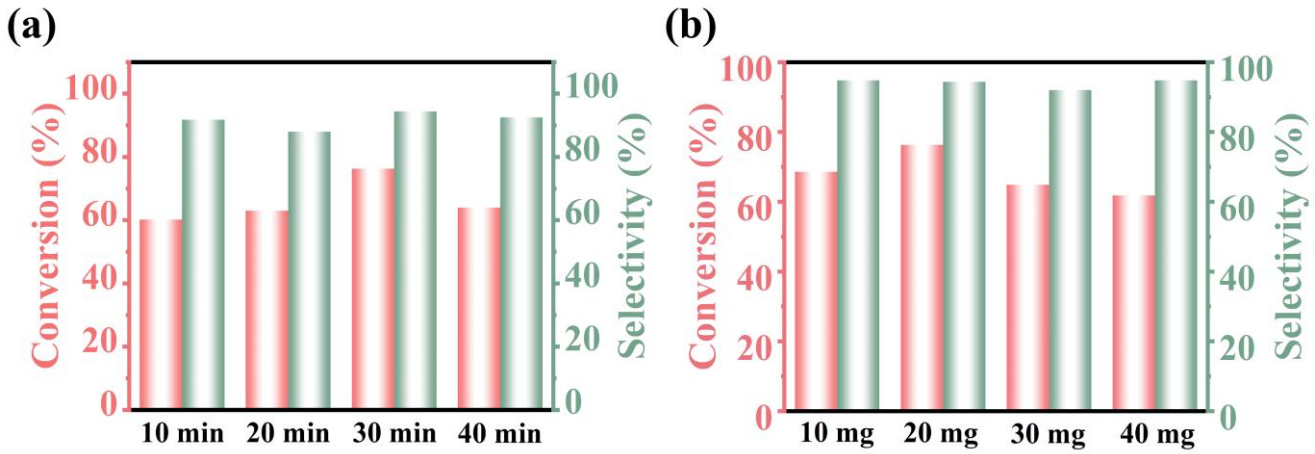

Figure S7 Conversion rate of furfuryl alcohol and selectivity of furfurylamine (a) different time of alkali etching, (b) different catalysts quality of CdS/CoAl(OH)$_x$-R.

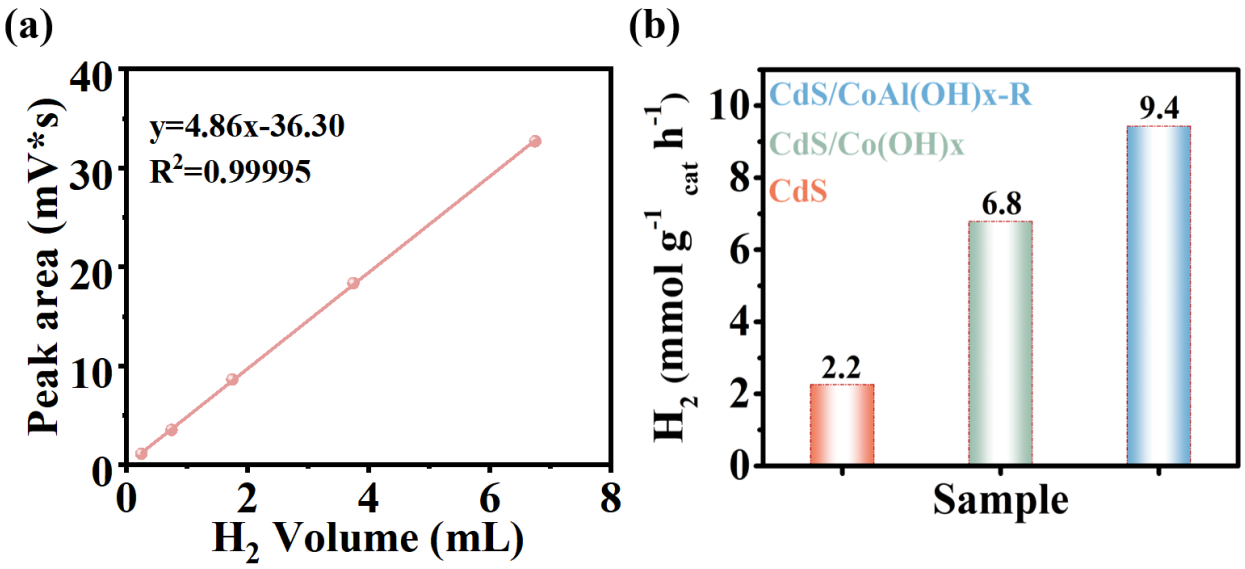

Figure S8 (a) Hydrogen standard curve. (b) The performance of photocatalytic H_2 production for different samples.

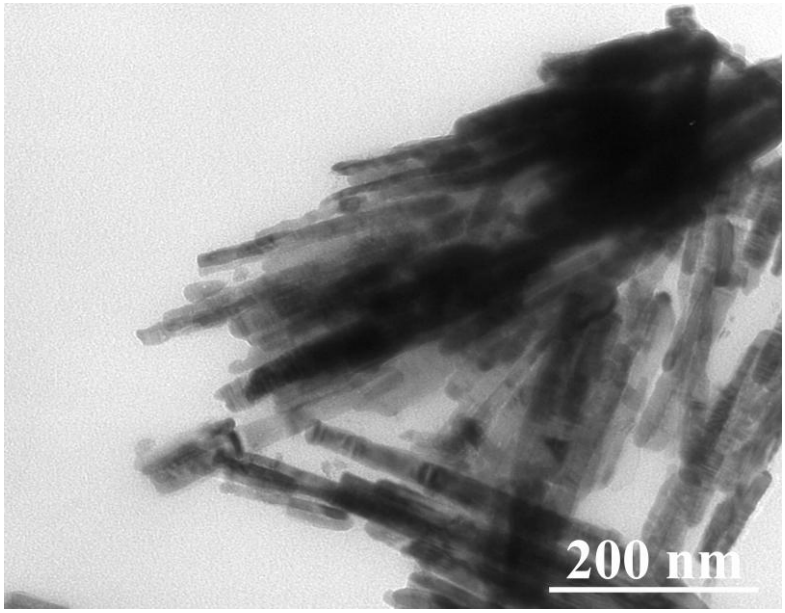

Figure S9 TEM images of CdS/CoAl(OH)$_x$-R after a long-term photoreforming.

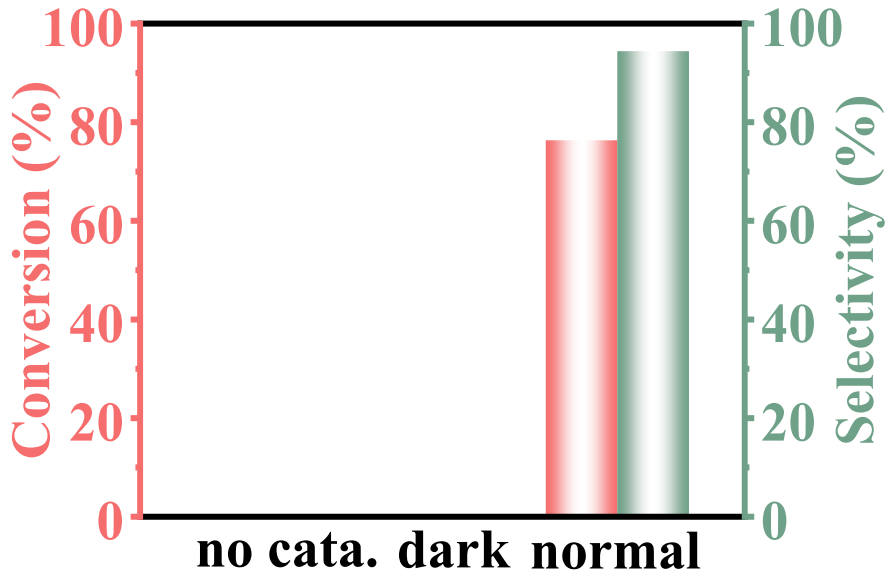

Figure S10 Photocatalytic conversion of furfuryl alcohol under different conditions.

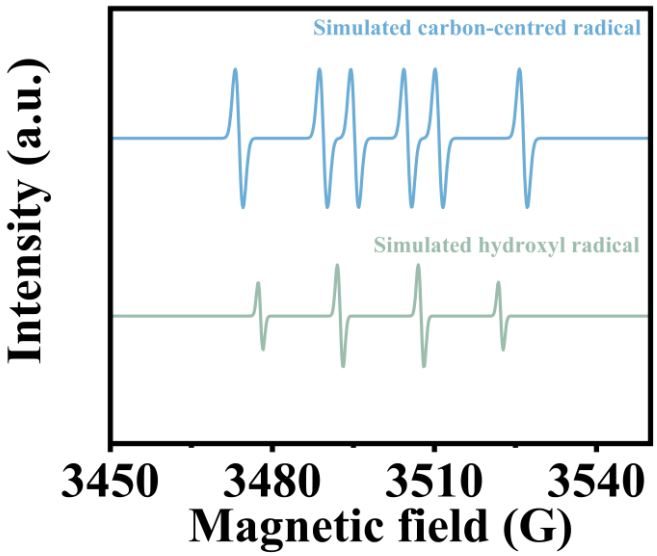

Figure S11 Theory signal value of free radicals.

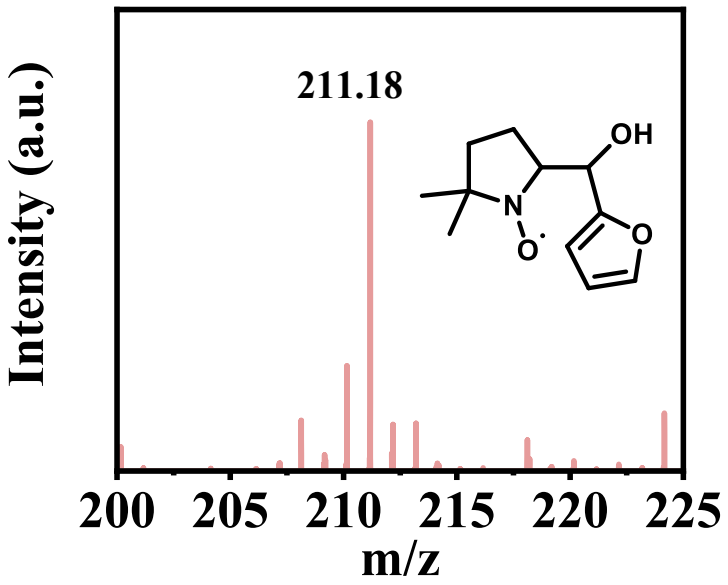

Figure S12 Positive-ion electrospray ionization mass spectrum in the presence of FFA and DMPO.

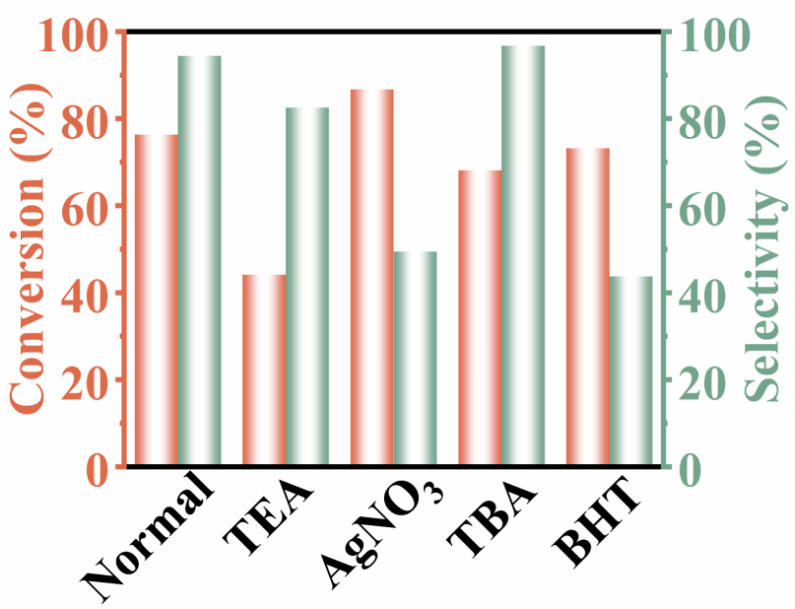

Figure S13 Control experiments with different scavengers.

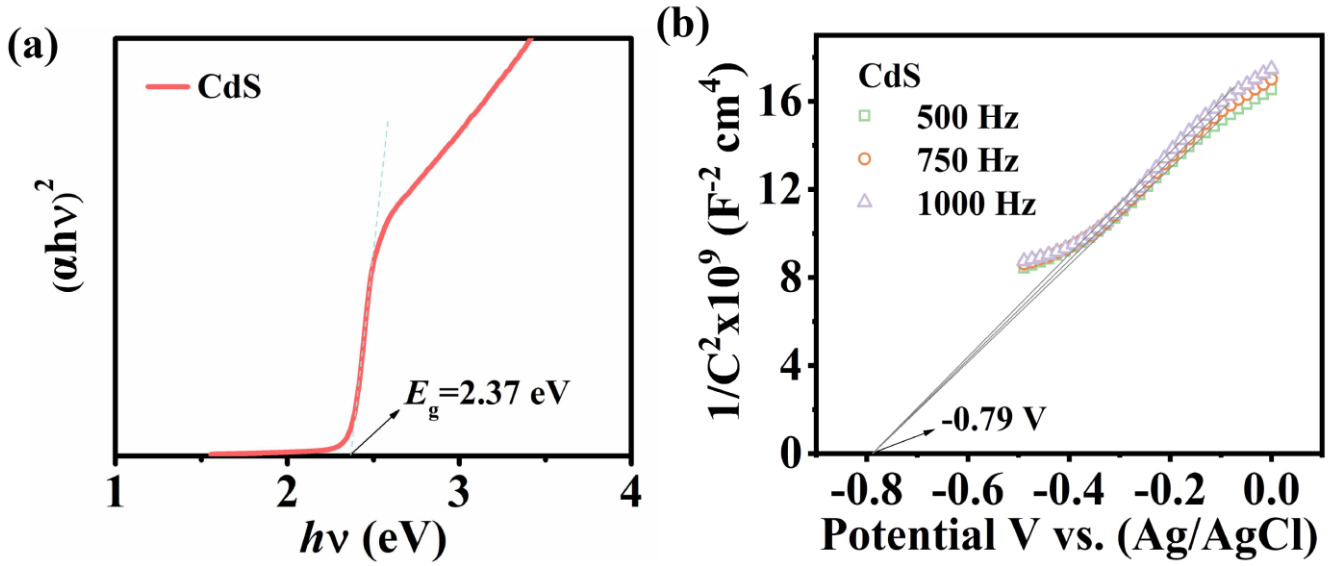

Figure S14 (a) Tauc plots and (b) Mott-Schottky plots of CdS.

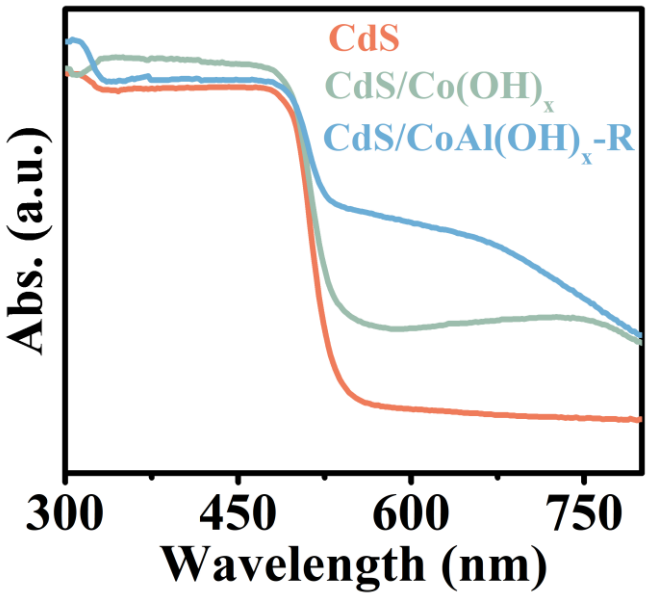

Figure S15 UV-vis diffuse reflectance spectra of different samples.

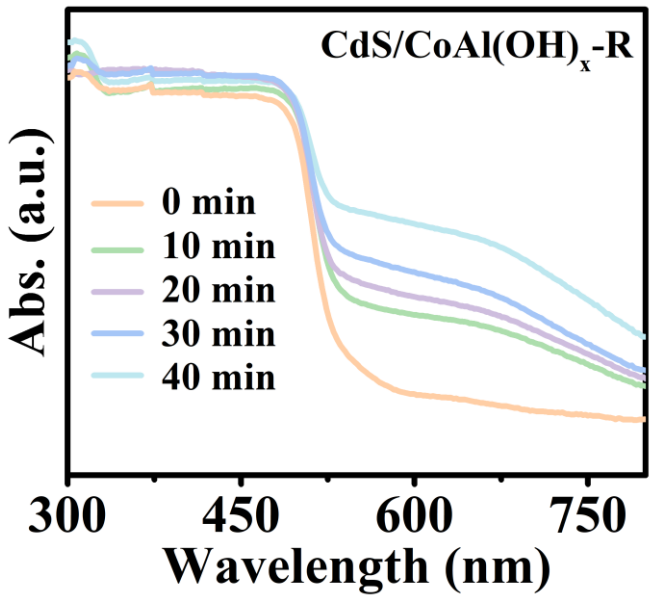

Figure S16 UV-vis diffuse reflectance spectra of CdS/CoAl(OH)$_x$ nanorods of different alkali etching time.

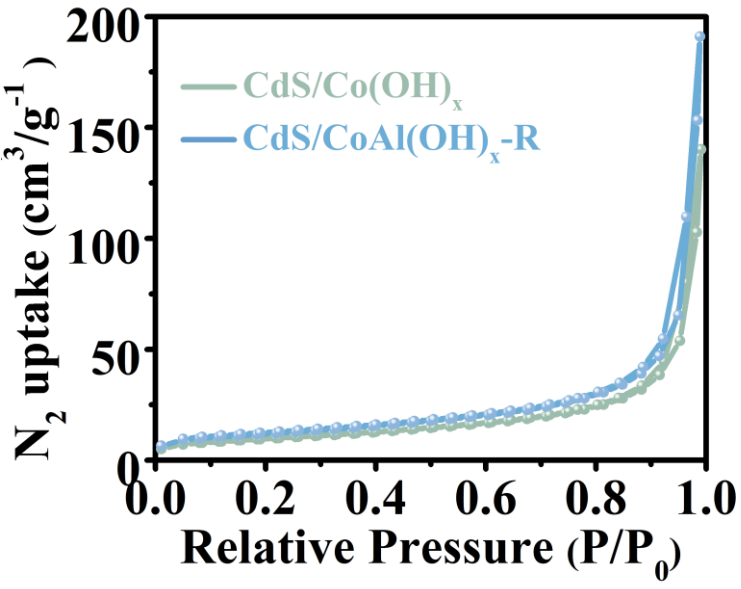

Figure S17 Nitrogen sorption isotherms of CdS/Co(OH)$_x$ and CdS/CoAl(OH)$_x$-R.

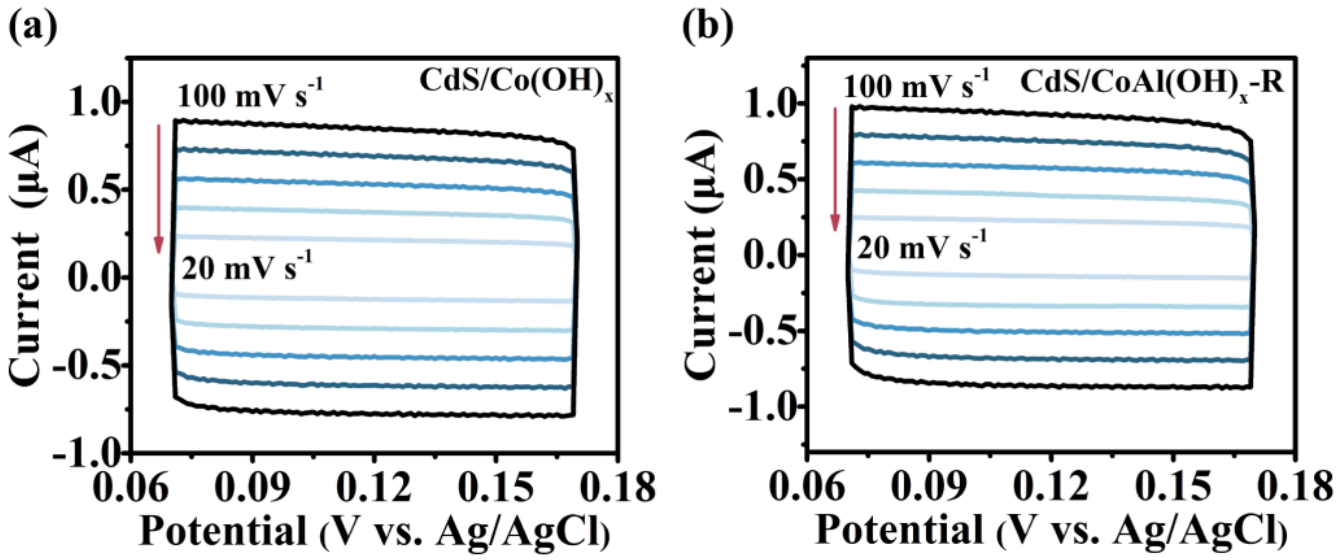

Figure S18 Cyclic voltammetry curves of (a) CdS/Co(OH)$_x$ and (b) CdS/CoAl(OH)$_x$-R measured at different scan rates.

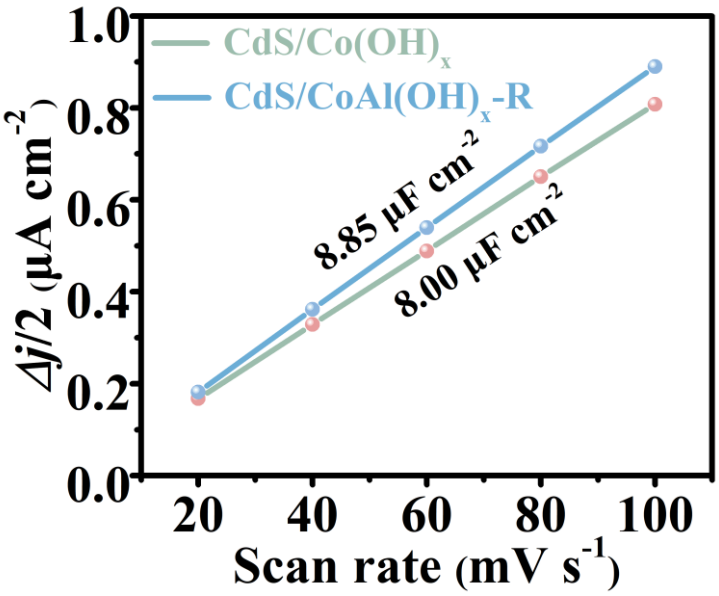

Figure S19 Plots of the electrochemical active surface areas (ECSA) for CdS/Co(OH)$_x$ and CdS/CoAl(OH)$_x$-R.

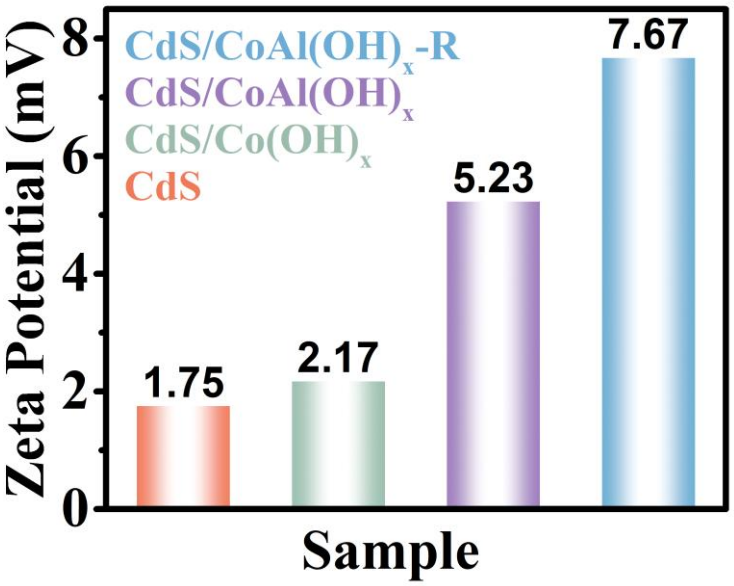

Figure S20 Zeta potential of different samples.

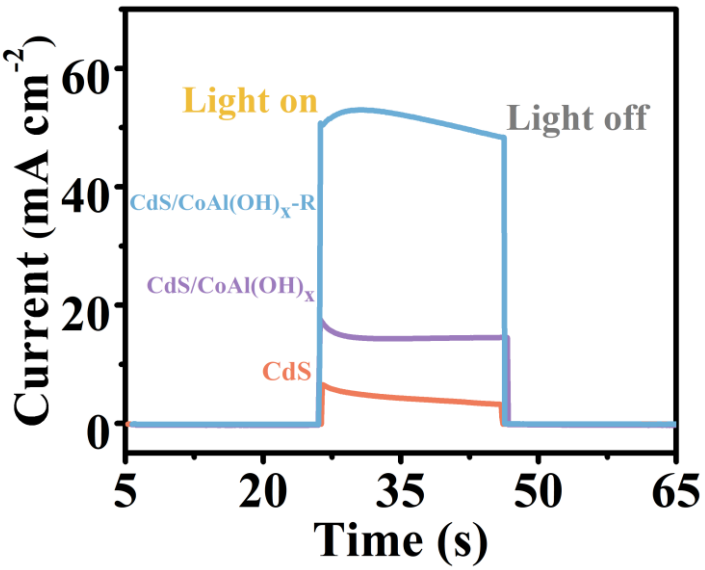

Figure S21 Transient photocurrent spectrum of CdS, CdS/Co(OH)$_x$, and CdS/CoAl(OH)$_x$-R in 0.5 M Na_2SO_4 using a 450 nm LED array.

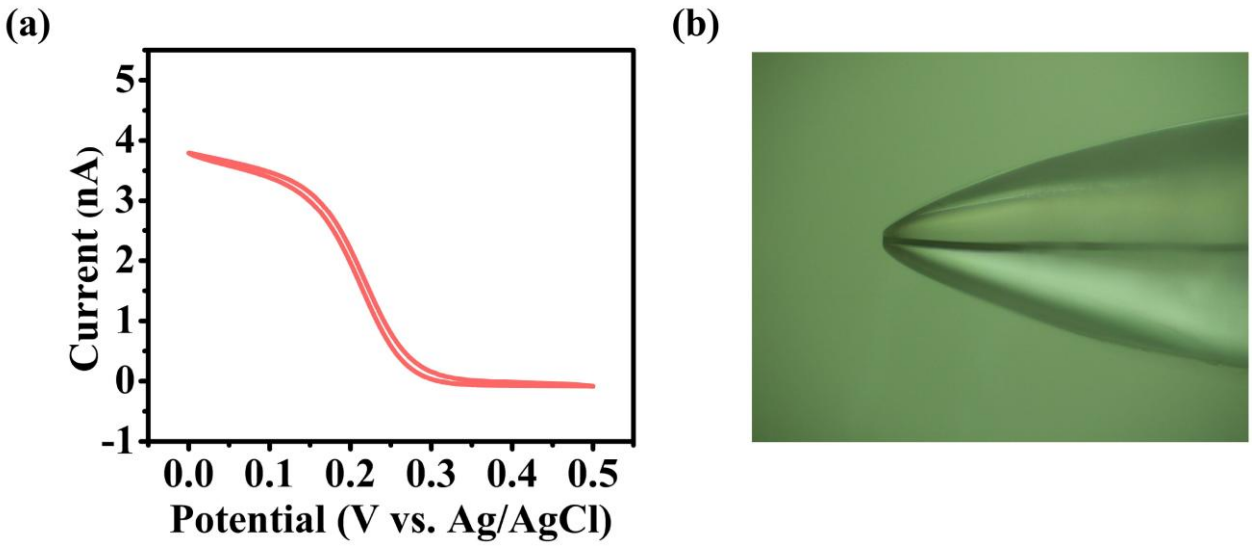

Figure S22 (a) Cyclic voltammograms of the ultra-microelectrode (UME) measured in 1 mM $K_3Fe(CN)_6$ containing 0.1 M KCl, (b) The image of the UME (RG ≈ 3).

Table S1 ICP-OES results of elements in CdS/CoAl(OH)$_x$-R with different alkali etching times.

Sample	Co (ppm)	Al (ppm)
CdS/CoAl(OH)$_x$	12.710	2.726
CdS/CoAl(OH)$_x$-R-10	11.078	0.079
CdS/CoAl(OH)$_x$-R-20	11.486	0.076
CdS/CoAl(OH)$_x$-R-30	11.655	0.063
CdS/CoAl(OH)$_x$-R-40	11.466	0.066
CdS/Co(OH)$_x$	12.297	0.017

Table S2 BET surface areas of $CdS/Co(OH)_x$ and $CdS/CoAl(OH)_x$-R.

Sample	Surface area ($m^2 g^{-1}$)
$CdS/Co(OH)_x$	34.8568
$CdS/CoAl(OH)_x$-R	42.5317

Table S3 Fitted parameters of TRPL for CdS, CdS/Co(OH)$_x$, and CdS/CoAl(OH)$_x$-R at 450 nm.

Sample	τ_1 (ns)	B_1	τ_2 (ns)	B_2	τ_{avg} (ns)
CdS	0.36	2859.54	4.63	9.39	0.53
CdS/Co(OH)$_x$	0.43	13407.10	4.01	57.36	1.08
CdS/CoAl(OH)$_x$-R	0.32	2566.79	3.11	17.83	2.27

Table S4 Kinetic parameters of CdS, CdS/$Co(OH)_x$ and CdS/$CoAl(OH)_x$-R obtained from open-circuit potential measurements.

Sample	K_r (s^{-1})
CdS	0.10889
CdS/$Co(OH)_x$	0.02913
CdS/$CoAl(OH)_x$-R	0.02036

Table S5 Catalytic performance in direct amination of furfuryl alcohol (FFA) to furfurylamine (FAM) over catalysts reported in literature.

Catalyst	Conversion of FFA (%)	Selectivity of FAM (%)	Reference
Ru/TiO_2 (5 wt% Ru)	72	53	S8
$Ni\text{-}Al_2O_3$ (50.5 wt% Ni)	48	90	S9
Raney Ni	27.8	29.9	S10
$Ni@Al_2O_3$ (5 wt% Ru)	21	94.3	S11
$CdS/CoAl(OH)_x$-R	76.32	94.78	This work

References

[1] J. Tao, M. Wang, X. Zhang, L. Lu, H. Tang, Q. Liu, S. Lei, G. Qiao, G. Liu, *Appl. Catal., B* **2023**, *320*, 122004.

[2] S. Niu, S. Li, Y. Du, X. Han, P. Xu, *ACS Energy Lett.* **2020**, *5*, 1083-1087.

[3] C.-X. Liu, K. Liu, Y. Xu, Z. Wang, Y. Weng, F. Liu, Y. Chen, *Angew. Chem. Int. Ed.* **2024**, *63*, e202401255.

[4] Y. He, R. Zhang, Z. Wang, H. Ye, H. Zhao, B. Lu, P. Du, X. Lu, *Anal. Chem.* **2024**, *96*, 110-116.

[5] B. Kang, M. Bilal Hussain, X. Cheng, C. Peng, Z. Wang, *J. Colloid Interface Sci.* **2022**, *626*, 146-155.

[6] W. Luo, H. Xiao, S. Zhang, Z. Wang, R. Zhang, J. Xue, Y. Feng, B. Lu, P. Du, X. Lu, *Angew. Chem. Int. Ed.* **2025**, e202504589.

[7] X. Ning, D. Yin, Y. Fan, Q. Zhang, P. Du, D. Zhang, J. Chen, X. Lu, *Adv. Energy Mater.* **2021**, *11*, 2100405.

[8] Y. Kita, M. Kuwabara, S. Yamadera, K. Kamata, M. Hara, *Chem. Sci.* **2020**, *11*, 9884-9890.

[9] K. Zhou, R. Xie, M. Xiao, D. Guo, Z. Cai, S. Kang, Y. Xu, J. Wei, *ChemCatChem* **2021**, *13*, 2074-2085.

[10] Y. Liu, K. Zhou, H. Shu, H. Liu, J. Lou, D. Guo, Z. Wei, X. Li, *Catal. Sci. Technol.* **2017**, *7*, 4129-4135.

[11] Y. Wei, H. Wang, Y. Qin, Y. Hu, J. Lin, S. Wan, S. Wang, *Chem. Eng. J.* **2024**, *491*, 151954.